Electrochimica Acta 58 (2011) 427–436

Contents lists available at SciVerse ScienceDirect

Electrochimica Acta

journal homepage: www.elsevier.com/locate/electacta

Experimental and theoretical studies for corrosion inhibition of carbon steel by imidazoline derivative in 5% NaCl saturated $Ca(OH)_2$ solution

Lijuan Feng, Huaiyu Yang*, Fuhui Wang

State Key Laboratory for Corrosion and Protection, Institute of Metal Research, Chinese Academy of Sciences, Shenyang 110016, China

ARTICLE INFO

Article history:
Received 18 July 2011
Received in revised form
23 September 2011
Accepted 23 September 2011
Available online 1 October 2011

Keywords:
Carbon steel
Corrosion inhibitor
Saturated $Ca(OH)_2$ solution
Quantum chemical calculation
Molecular dynamic simulation

ABSTRACT

The inhibition activity of an imidazoline derivative, namely 1-[N,N′-bis(hydroxylethylether)-aminoethyl]-2-stearicimidazoline (HASI) for carbon steel in 5% NaCl saturated $Ca(OH)_2$ solution was investigated using electrochemical measurements in conjunction with Raman and Fourier transform infrared (FTIR) spectroscopy techniques. Quantum chemical calculations and molecular dynamic (MD) simulations were applied to analyze the experimental data and elucidate the adsorption behavior and inhibition mechanism of inhibitor. The results indicate that HASI is an effective inhibitor in protecting carbon steel from corrosion in alkaline chloride solution and acts as a cathodic type inhibitor with the dominant suppression of cathodic reduction of oxygen. The inhibition behavior of HASI is strongly related to its adsorption activity on carbon steel surface, which leads to an enhancing in the corrosion resistance of carbon steel and a reduction in the corrosion rate. Density functional theory (DFT) calculations suggest that the N=C–N region in imidazoline ring is the most active reaction site for the inhibitor adsorption on metal surface via the donor–acceptor interactions between the lone electron pairs on nitrogen atoms together with the π-electrons of heterocyclic and the vacant d orbital of iron atoms. The adsorption of inhibitor on three typical surfaces (Fe (1 0 0), F_2O_3 (1 1 0) and F_3O_4 (1 0 0)) takes nearly parallel to the surface so as to maximize its contact with the surface, as shown as the MD simulations. The experiments incorporating the theoretical calculation and MD simulation can provide an insight into the understanding of interactions between the inhibitor molecules and the carbon steel surfaces.

1. Introduction

Reinforced concrete structures are widely used in various construction fields due to their excellent structural performance and durability [1–3]. However, there are many instances of premature failure of reinforced concrete components worldwide because of the reinforcement corrosion, which has become a serious problem and resulted in the huge socio-economic impact for some industrial departments [4,5]. Generally, there are two factors causing the corrosion of steel rebar embedded in concrete. One is the CO_2 in the air which reacts with the alkaline components in concrete resulting in the decrease of pH and consequently the loss of passivation of reinforcing steel. The other one is chloride ions which penetrate to the concrete and ingress into the passive layer leading to the localized or pitting corrosion of reinforcing steel [6–8].

In order to reduce or eliminate the reinforcement corrosion, several methods have been used, including coating, cathodic protection, corrosion inhibitors and a combination of these above techniques [9–11]. Among them, the application of corrosion inhibitors is envisaged as an effective and economical solution [4,6,8–14]. Nitrite-based inhibitors are considered as the most effective additives available on the market for the protection and prevention of reinforcement corrosion [4,10]. However, owing to the strict environmental restricts, the traditional inorganic inhibitors which have been proved to be of great help for extending the service life of reinforced concrete structure are forbidden by more and more countries [15,16]. Therefore, it is necessary to develop environmental-friendly corrosion inhibitors to replace the inorganic salts, either partially or totally.

The existing data suggest that the organic compounds with functional groups such as $-NH_2$, –OH, –SH, –COOH, $-SO_3H$ and ring structure containing hetero atoms may be potential inhibitors because they can interact with metals to form a protective film on the metal surface [3,6,10,15]. Moreover, some organic compounds such as amino acids, ascorbic acid, polyepoxysuccinic acid, and imidazoline compounds as well as their derivatives have also been claimed to be environmental-friendly [17–20]. In recent years, hence, an increasing interest has been focused on the investigation of inhibition behavior of some new organic compounds for the reinforcement corrosion and the understanding of their inhibition mechanism [17,21–27]. Generally, the organic inhibitors for chloride reduced corrosion can act by [4,6,15,17]: (i) forming a

* Corresponding author. Tel.: +86 24 23915899; fax: +86 24 23893624.
E-mail address: hyyang@imr.ac.cn (H. Yang).

0013-4686/$ – see front matter © 2011 Elsevier Ltd. All rights reserved.
doi:10.1016/j.electacta.2011.09.063

film to block the adsorption of chloride ions and consequently to inhibit the anodic, cathodic or both reactions, (ii) competitive surface adsorption processes between inhibitor and chloride ions or competitive migration of inhibitor and chloride ions into the pit, (iii) leading to an increase in the chloride threshold value, and (iv) repairing defects or pores in the film to mitigate further corrosion. However, a perusal of literatures reveals that there are still conflicting opinions on the effectiveness of these inhibitors on the steel rebar, and there is very little information on the mechanism by which these organic substances exhibit their inhibitive action [4,6,10,21–27]. For example, some authors reported that the alkanolamine-based inhibitors can form a monomolecular protective layer to reduce the reinforcement corrosion by retarding both the anodic and cathodic processes of steel rebar [28–31], whereas other researchers found that they are not effective or have the low inhibition efficiencies when concrete is under immersion conditions [32–34]. Furthermore, many inhibitors have been claimed only be effective when the chloride content is low, in the aggressive condition such as marine environments, they seem to be not so useful [1,10].

In order to elucidate the inhibition mechanism of organic inhibitors, the investigation on the molecular configuration, electronic structure, reactivity of the inhibitors and the interactions that happened between the adsorbed inhibitor molecules and the metal surface is essential. Quantum chemical calculation and molecular dynamic simulation are the most appropriate methods to achieve this purpose [35]. Based on these techniques, the correlation of the inhibitor molecular structure and its ability to inhibit the corrosion process can be obtained, and the inhibition mechanism can be directly accounted for in terms of the chemical reactivity of the compounds under study as well [35–37]. Quite recently, the Materials Studio Modeling 4.0 software (developed by Accelrys Co.) has proven to be very useful in determining the quantum chemical parameters of organic inhibitor molecules as well as in clarifying the interactions of inhibitor with the metal surface based on the density function theory (DFT) with the DMol3 and Discover module in the software package. Especially in the study of adsorption behavior of inhibitors, much achievement was reached using this software [36,38–40].

In this paper, the saturated $Ca(OH)_2$ solutions was used to simulate the concrete pore solution, 5% NaCl was added to create the aggressive condition. The inhibition activity of a commercial imidazoline derivative (labeled as HASI and shown in Fig. 1) for the carbon steel was investigated by electrochemical measurements, surface analysis, quantum chemical calculations and molecular dynamic simulation. The aim of the work is to assess the inhibition performance of this inhibitor on the corrosion of carbon steel in alkaline chloride solution and examine its inhibition mechanism, furthermore, to elucidate the possible adsorption model on the corroding carbon steel surface and advance the understanding of interactions between the inhibitor molecules and the carbon steel surfaces.

2. Experimental

2.1. Materials and sample preparation

The test solution was 5% NaCl (wt%) saturated $Ca(OH)_2$ solution prepared from reagent grade chemicals and bi-distilled water. The inhibitor tested was a type of stearic imidazoline derivatives, which was purchased from Yixing Chemical Co. as high grade reagent and used without further purification. The employed concentration range of inhibitor was 0.19–1.89 mM. The molecular structure is depicted in Fig. 1.

All the working electrodes (⌀ 8 mm × 10 mm) were cut from the steel rebar (0.15% C; 0.15% Si; 0.44% Mn; 0.30% P; 0.03% S and balance Fe). Except for an exposed area of 0.502 cm^2, the rest part was embedded in epoxy resin. Prior to experiments, all specimens were gradually ground with emery paper to 800 grit, then washed with distilled water, degreased in acetone and dried with cool air. All experiments were conducted at room temperature.

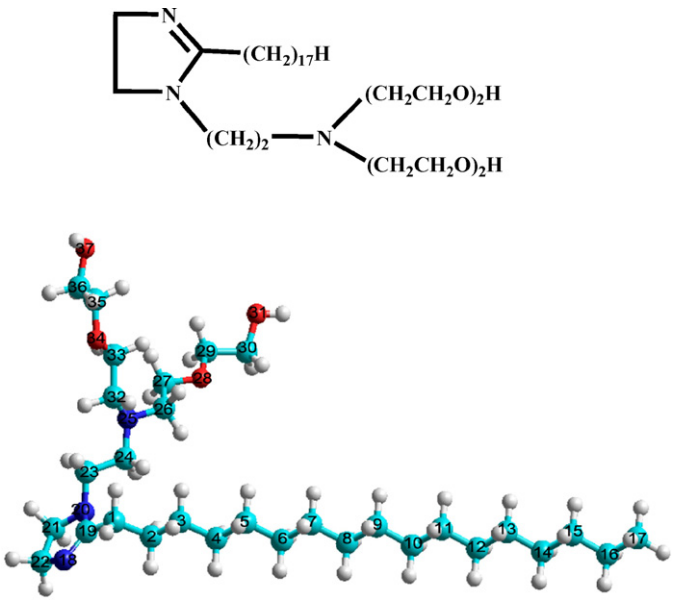

Fig. 1. The molecular formula and the optimized molecular structure of HASI.

2.2. Electrochemical measurements

Electrochemical tests were performed on the Parstat 2273 system (Princeton Applied Research) facilitated with a three-electrode jacketed test instrument. A large platinum plate (2 cm × 2 cm) was used as the counter electrode. The reference electrode was saturated KCl calomel electrode (SCE) coupled with a Luggin capillary, the tip of which was located about 3 mm away from the working electrode to reduce the ohmic drop.

Except the open circuit potential (OCP) experiments, all of the electrochemical measurements were conducted after 3 days immersion in test solutions with and without the addition of an inhibitor, which allowed the working electrode to reach a stable state (the OCP fluctuation was less than ±10 mV). The linear polarization resistance (LPR) tests were performed in the range −20 mV to +20 mV versus OCP with the scan rate of 0.166 mV s^{-1}. The potentiodynamic polarization curves were obtained from −250 mV versus OCP to the potential at which the current density increased abruptly with a scan rate of 1 mV s^{-1}. The electrochemical impedance spectra (EIS) were collected in the frequency range 100 kHz to 10 mHz at the OCP using a 10 mV sinusoidal potential perturbation, with five points per decade. The cyclic voltammetry curves were recorded in the scan range of −1.2 to −0.1 V (SCE) with a scan rate of 20 mV s^{-1}. All electrochemical experiments were carried out under open to air conditions. Each sample was only used in one electrochemical test.

2.3. Surface observation and analysis

After the measurement of open circuit potential, the sample surface was directly observed by scanning electron microscope (Philip XL30).

Before each experiment, the carbon steel sample was roughened down to 2.5 μm and immersed in the test solutions with and without the inhibitor for 3 days, and then the Raman spectra were

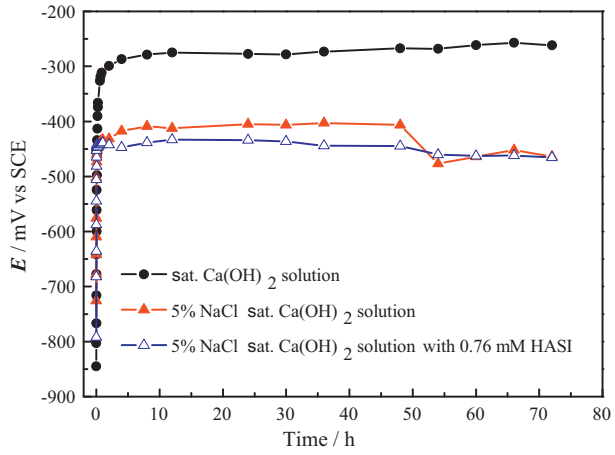

Fig. 2. Evolution of open circuit potential for carbon steel samples immersed in different solutions.

conducted using a confocal microprobe Raman system (JY HB800) with the excitation laser line of 632.8 nm at the range of 200 and 1800 cm^{-1}. The FTIR spectra (Nicolet 560) were collected between 650 and 4000 cm^{-1} at the single reflection mode.

2.4. Quantum chemical calculation and molecular simulation

Quantum chemical calculations and molecular simulations were performed by Materials Studio Modeling 4.0 software (Accelrys Co.). The molecular structure of the inhibitor was fully geometrically optimized by DMol3 module using density functional theory to produce highly accurate results of the molecular structure in a relative short time.

Then the Discover program was used to simulate the interactions between the inhibitor molecules and the iron or oxide-covered iron surfaces by classical molecular dynamics (MD) method with COMPASS force field. Considering the presence of iron oxides on the sample surface after 3 days immersion, three typical surfaces, i.e. Fe (1 0 0), F_2O_3 (1 1 0) and F_3O_4 (1 0 0) were chosen to simulate the adsorption process of the inhibitor molecules since they have the least lattice mismatch. The interactions between inhibitor molecules and Fe (1 0 0), F_2O_3 (1 1 0) and F_3O_4 (1 0 0) surfaces were simulated in boxes of 22.93 Å × 28.66 Å × 37.17 Å, 26.16 Å × 27.44 Å × 36.80 Å and 23.74 Å × 29.67 Å × 38.35 Å, respectively. The periodic boundary conditions were applied in all three directions and the equations of motion were integrated within the canonical ensemble NVT. Nose method was used to control the temperature (T = 298 K) with an integration time of 1 fs. The MD simulation was stopped until the temperature fluctuation was less than 10 T and the energy deviation was less than 0.2%.

3. Results and discussions

3.1. Electrochemical measurements

3.1.1. OCP measurements and surface observation

For determining the effects of NaCl and inhibitor addition on the corrosive behavior of carbon steel in saturated $Ca(OH)_2$ solution, Fig. 2 depicts the evolution of open circuit potential with immersion time for carbon steel samples exposed to different solutions. It is clear that the OCP immediately after immersion was very negative for all the cases, and then it increased rapidly to reach a more positive value with immersion time due to the high alkalinity of the test electrolyte. With the further increasing of immersion time, the OCP gradually reached the steady state value (about −270 mV versus SCE) for the saturated $Ca(OH)_2$ system, which could be associated with the formation of a more oxidized passive layer and indicates that the carbon steel is in the passive state [41–43]. However, in the 5% NaCl saturated $Ca(OH)_2$ solution, the OCP reached a stable value after 8 h immersion and maintained almost constant until 48 h, after that it shifted abruptly to most negative values and then was likely stabilized (about −450 mV versus SCE). This shift of potential suggests the loss of passivation of carbon steel surface due to the chloride ion attack and the electrode is in the active state [11,15,44]. For the system of 5% NaCl saturated $Ca(OH)_2$ solution with the inhibitor, the potential decreased slowly to more negative values with increasing of immersion time and then reached the stabilization after 54 h. The continuous shift of potential to the cathodic direction can be attributed to the spontaneous adsorption of inhibitor on carbon steel surface, suggesting the inhibitor may be has a cathodic inhibition effect.

Fig. 3 exhibits the surface morphologies of carbon steel samples after 3 days immersion in different solutions. It can be seen that in the saturated $Ca(OH)_2$ solution, the carbon steel surface was smooth and no noticeable corrosion sign was observed, whereas in the 5% NaCl saturated $Ca(OH)_2$ solution, the carbon steel surface was seriously damaged by the localized corrosion. However, in the presence of inhibitor in the 5% NaCl saturated $Ca(OH)_2$ solution, the specimen surface was almost as smooth as in the saturated $Ca(OH)_2$ solution, indicating the corrosion of carbon steel was strongly restricted by the inhibitor.

Thus, it can be concluded that in the present study, the carbon steel surface can be kept in the passive state due to the high alkalinity of saturated $Ca(OH)_2$ solution. However, in the presence of 5% NaCl, the carbon steel will lose the passivity and be in the active corrosion state because of the attack of chloride ions. The addition of an inhibitor can effectively retard the corrosion by adsorption on carbon steel surface, probably forming a protective adsorption film in which involved some iron oxides and hydroxides.

3.1.2. LPR, potentiodynamic measurements and Raman spectra analysis

For obtaining a well understanding on the inhibition mechanism, the inhibition behavior of HASI for carbon steel in 5% NaCl saturated $Ca(OH)_2$ solution was further studied by the LPR and potentiodynamic polarization. Fig. 4 presents the potentiodynamic polarization curves for carbon steel after 3 days immersion in test solutions without and with various concentrations of the inhibitor. Table 1 collects the relevant electrochemical parameters obtained from the potentiodynamic polarization and LPR measurements. The corrosion efficiency (η_{LPR}) was calculated according to the following equation [45]:

$$\eta_{LPR}\ (\%) = \left(1 - \frac{R_p^0}{R_p}\right) \times 100 \quad (1)$$

where R_p^0 and R_p are the polarization resistances of the carbon steel electrodes in the uninhibited and the inhibited solution, respectively.

It can be seen from Fig. 4 that the presence of inhibitor strongly decreased the cathodic corrosion current densities and resulted in a negative shift of the corrosion potential (E_{corr}), while the anodic corrosion current densities were reduced with increasing concentrations of the inhibitor. These results suggest that the inhibitor has a stronger inhibition effect on the cathodic oxygen reduction than the anodic dissolution of iron, and the compound acts as a cathodic type inhibitor. This inhibition effect can be ascribed to the surface structure change due to the inhibitor molecules being adsorbed on the carbon steel surface. The shape of polarization curve in all cases was similar, indicating that the addition of the inhibitor did not change the anodic and cathodic reaction mechanism.

Table 1
Electrochemical parameters obtained from the potentiodynamic polarization and linear polarization data for carbon steel electrodes in 5% NaCl sat. $Ca(OH)_2$ solutions without and with various concentrations of inhibitor.

Conc. (mM)	E_{corr} (mV versus SCE)	i_{corr} ($\mu A\,cm^{-2}$)	$-\beta_c$ ($mV\,dec^{-1}$)	β_a ($mV\,dec^{-1}$)	R_p ($k\Omega\,cm^2$)	η_{LPR} (%)
Blank	−512	2.41	62	74	6.48	
0.19	−614	0.98	65	75	14.6	55.6
0.38	−630	0.72	66	78	19.3	66.4
0.76	−641	0.60	78	81	23.9	72.9
1.89	−661	0.35	82	84	34.4	81.2

Moreover, it also can be seen from Fig. 4 that when the anodic polarization potential moved to more positive potential, the pitting was accompanied by a sharp current density increase for all cases, and all the pitting initiation potentials measured on the carbon steel in alkaline chloride solutions without and with the inhibitor were below the oxygen evolution potential. These reveal that the occurrence of pitting was initiated by the Cl^- attack rather than the effect of local OH^- depletion on the electrode surface. These results are in good agreement with those reported in publications [11,22].

Table 1 clearly shows that by increasing inhibitor concentrations, the corrosion current densities decreased, while both the polarization resistances and inhibition efficiencies increased. These suggest that the inhibition effect of HASI on the carbon steel corrosion in alkaline chloride solution is dependent on the inhibitor concentration and the amount of inhibitor molecules adsorbed on carbon steel surface increases with increasing concentrations of the inhibitor. A definite negative shift of the E_{corr} indicates the inhibitor behaved as a cathodic type inhibitor with the dominant control of cathodic oxygen reduction reaction [46].

Previous studies [47–49] demonstrated that in alkaline solution, the compositions of oxides formed on iron surface play an important role in the cathodic reduction process of oxygen. In order to further understand the effect of inhibitor on the cathodic oxygen reduction, the cyclic voltammetry curves were recorded in 5% NaCl saturated $Ca(OH)_2$ solutions without and with 0.76 mM HASI, as shown in Fig. 5.

It is evident that in the blank solution, the overlapping anodic peaks at −0.63 V and −0.61 V can be observed during the anodic scan process, which can be assigned to the oxidation reactions from ferrous compounds (also probably comprise partial ferric species) to ferric oxides and/or hydroxides, as reported before [50–52]. In the backward scan, the reduction peaks of ferric species to ferrous ones can also be clearly resolved. However, after the addition of an inhibitor, it is apparent that during the forward scan process, the corresponding oxidation peaks became smaller compared with that in blank solution, while the anodic current density decreased. This suggests that the adsorbed inhibitor molecules on electrode surface not only effectively retarded the anodic dissolution of iron, but also enhanced the stability of ferrous species to be further oxidized (Fe^{2+} only) into ferric ones.

Fig. 6 depicts the Raman spectroscopy for carbon steel samples after 3 days immersion in test solutions without and with 0.76 mM HASI. Because of the Raman signs were weak at low inhibitor concentrations, here only the Raman spectroscopy at high inhibitor concentration is presented. It can be seen that for the blank solution, a strong peak at 509 cm^{-1} was observed with a smaller band at 375 cm^{-1}, which can be assigned to the ferrihydrite due to Fe^{3+} oxides and hydroxides are the most poorly ordered and crystallized form [50,51,53]. This indicates that in the blank solution, the corrosion products formed on the carbon steel surface mainly consist of ferric oxides and/or hydroxides. However, in the presence of inhibitor, only one weak peak at 668 cm^{-1} appeared in the spectrum, which can be assigned to the Fe_3O_4 [50,51,53]. These results reveal that the addition of an inhibitor largely restricted not only the formation of ferrous compounds, but also the further oxidization of ferrous species into ferric ones by the adsorption interactions with the oxides on the carbon steel surface, subsequently preventing the precipitation as the Fe^{3+} species. This is consistent with that obtained from the cyclic voltammetry.

Based on the above results, it is reasonable to interpret why HASI acted as a cathodic type inhibitor. It is pointed out that in alkaline solution, the octahedrally coordinated surface ferrous ions [Fe(II)OH^-] are the electrocatalysis active centers for the cathodic reduction of oxygen on the oxide-covered iron surface [48]. In the inhibited solution, the inhibitor can largely reduce the formation of iron oxides and hydroxides due to the covering of adsorbed inhibitor molecules on the carbon steel surface, resulting in the reduction in the amount of active sites. In addition, the HASI molecules can also preferably adsorb on these active sites, blocking the direct contact of oxygen dissolved in solution with the ferrous ions. Hence, the cathodic reduction reaction of oxygen is suppressed by the adsorbed inhibitor molecules according to the catalytic mechanism which is completely described by E.J. Calvo [47–49].

3.1.3. Electrochemical impedance spectroscopy

Fig. 7 shows the complex-plane impedance and Bode plots for carbon steel in alkaline chloride solutions without and with various concentrations of the inhibitor. As would be expected in the blank solution, a large decrease of the impedance modulus was obtained, which reveals an increase in the corrosion rate on carbon steel surface due to the presence of chloride ions in test solution. However, after the addition of an inhibitor, the impedance modulus of the electrodes gradually increased by increasing concentrations of the inhibitor, the low frequency limit of the impedance was nearly one order of magnitude greater than that in the blank solution when the inhibitor concentration was 1.89 mM. These results indicate that the development of protective adsorption film on electrode surface due to the increasing in amount of inhibitor molecules adsorbed on electrode surface and the corrosion of carbon steel was effectively retarded by the inhibitor [14,44,54].

It is well known that in alkaline solution, a two-layer oxide film consisting of an inner barrier layer and an outer porous layer is present on the carbon steel surface. The corrosion rate of carbon steel is mainly dependent on the property of the barrier layer. According to the reports in the literature, the corresponding impedance spectra for carbon steels in alkaline chloride solution are composed of two time constant [17,23,42–44]. The one at high frequencies is associated with the behavior of the protective film formed on electrode surface, which consists of the adsorbed inhibitor molecules, iron oxides and hydroxides. The other one at low frequencies is related to the charge transfer reactions occurring in pores and defects of the protective film that determines the redox process of iron, as described in the previous papers [15,44,54]. Owing to the forming of a more compact and stable protective adsorption film with HASI on the electrode surface, a wide and high phase angle region appeared at the middle frequency range, as shown in Fig. 7b. Based on the above facts and practice state of carbon steel electrodes, the impedance results can be interpreted by the equivalent circuit shown in Fig. 8, which has been successfully used to analyze EIS data for steel in alkaline electrolytes in the literature [15,44,54–58]. In this circuit, R_s represents the

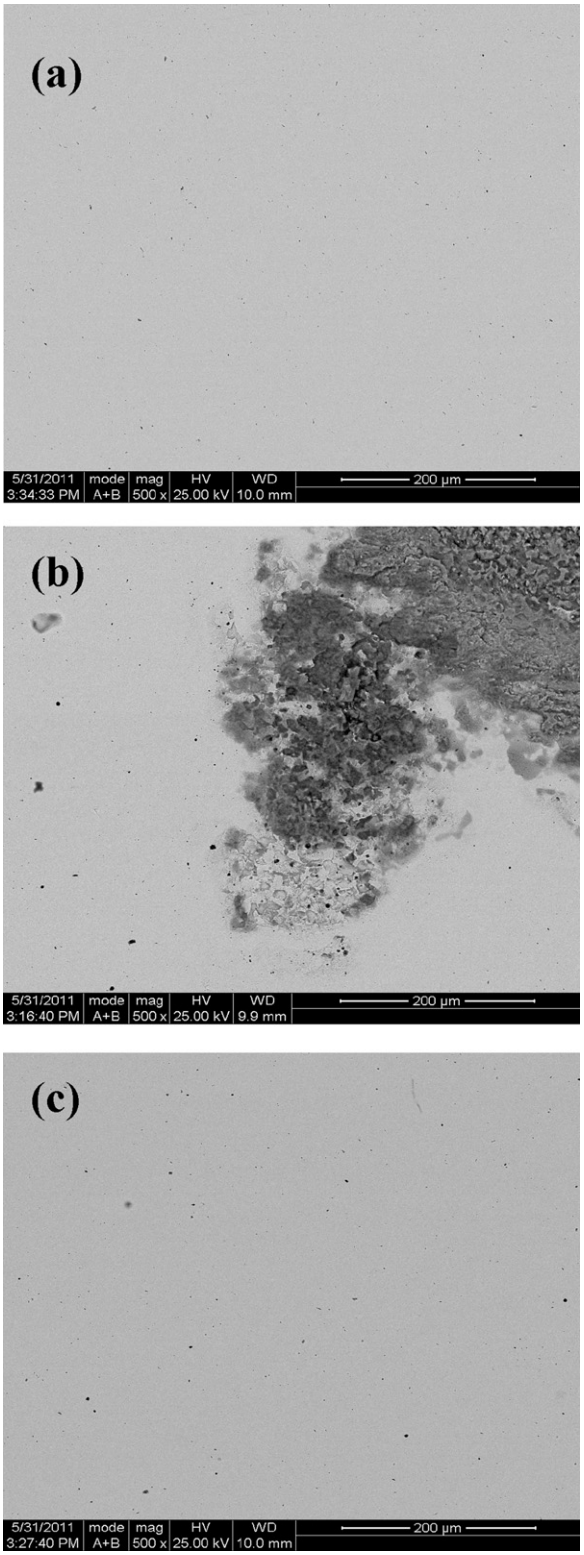

Fig. 3. SEM images for carbon steel samples after 3 days immersion in different solutions: (a) sat. $Ca(OH)_2$ solution; (b) 5% NaCl sat. $Ca(OH)_2$ solution; (c) 5% NaCl sat. $Ca(OH)_2$ solution with 0.76 mM inhibitor.

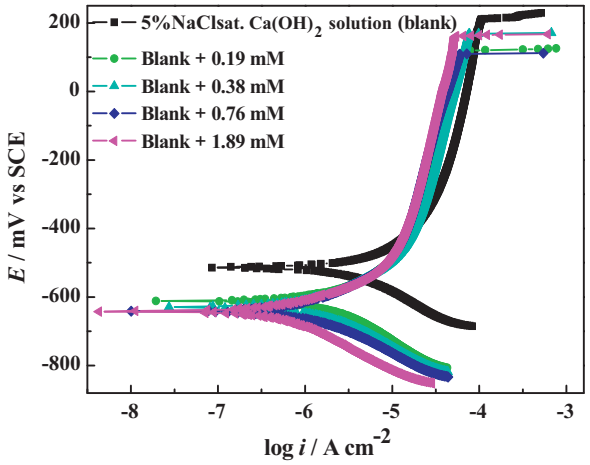

Fig. 4. Polarization curves for carbon steel in 5% NaCl sat. $Ca(OH)_2$ solutions without and with different concentrations of inhibitor.

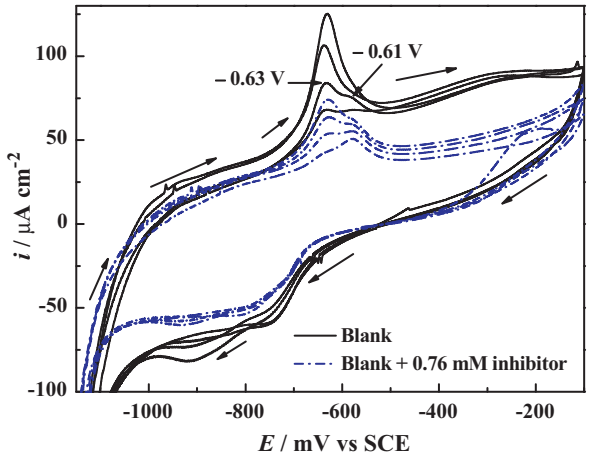

Fig. 5. Cyclic voltammetry curves (1st–4th cycle) for carbon steel electrode immersed in 5% NaCl sat. $Ca(OH)_2$ solutions without and with 0.76 mM inhibitor.

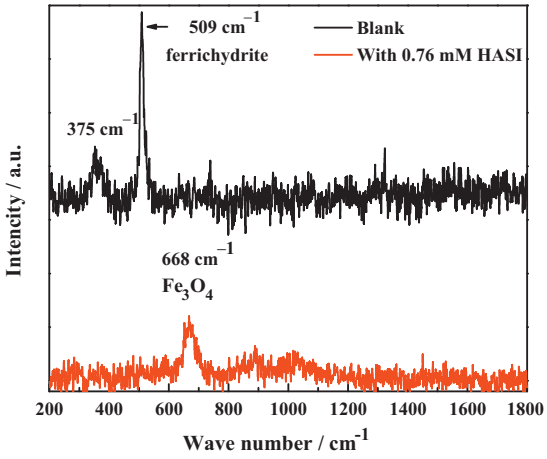

Fig. 6. Raman spectra for carbon steel examples after 3 days immersion in 5% NaCl sat. $Ca(OH)_2$ solutions without and with 0.76 mM inhibitor.

solution resistance, R_f is the film resistance, R_{ct} represents the charge transfer resistance of the electric double layer. Considering the roughness and in-homogeneities of solid electrode surface, here, the constant phase elements CPE_1 and CPE_2 are used to replace the film capacitance and the double layer capacitance, respectively, and the value can be assessed by the following equation [59,60]:

$$Z_{CPE}(\omega) = Y_0^{-1}(j\omega)^{-n} \quad (2)$$

Table 2
Electrochemical parameters obtained from the EIS data for carbon steel electrodes in 5% NaCl sat. $Ca(OH)_2$ solution without and with various concentrations of inhibitor.

Conc. (mM)	R_s (Ω cm^2)	CPE_1		R_f (kΩ cm^2)	CPE_2		R_{ct} (kΩ cm^2)	η_{EIS} (%)
		Y_{0-CPE_1} ($\mu\Omega^{-1}$ S^n cm^{-2})	n_1		$Y_{0\text{-}CPE_2}$ ($\mu\Omega^{-1}$ S^n cm^{-2})	n_2		
Blank	8.6	52.7	0.80	1.23	909	0.57	6.26	
0.19	10.3	31.6	0.81	3.16	311	0.48	12.8	51.1
0.38	8.8	27.5	0.82	3.84	216	0.42	18.3	65.8
0.76	9.7	25.8	0.80	4.95	164	0.41	22.3	71.9
1.89	10.6	24.5	0.80	7.53	157	0.47	34.6	81.9

where Y_0 is the CPE constant, ω is the angular frequency (in rad/s), $j^2 = -1$, is the imaginary number and n is the CPE exponent. Depending on n, CPE can represent resistance [$Z_{CPE} = R$, $n = 0$], capacitance [$Z_{CPE} = C$, $n = 1$], inductance [$Z_{CPE} = L$, $n = -1$] or Warburg impedance for ($n = 0.5$) [44,61]. The associated impedance parameters are listed in Table 2, where the inhibition efficiency (η_{EIS}) was calculated by following equation [12]:

$$\eta_{EIS}\ (\%) = \frac{R_{ct} - R_{ct}^0}{R_{ct}} \times 100 \quad (3)$$

where R_{ct}^0 and R_{ct} are the charge transfer resistances in the uninhibited and the inhibited system, respectively.

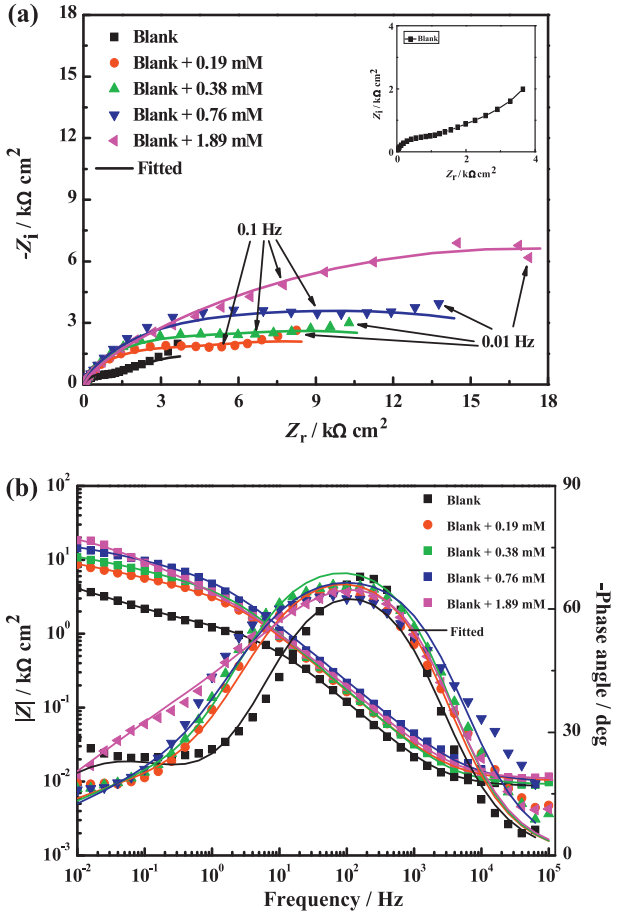

Fig. 7. Complex-plane impedance (a) and Bode (b) plots for carbon steel electrodes exposed to 5% NaCl sat. $Ca(OH)_2$ solutions with different concentrations of inhibitor.

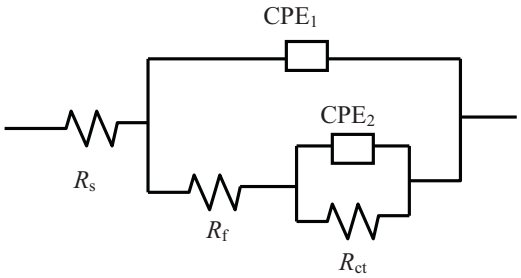

Fig. 8. The equivalent circuit for impedance analysis.

Fig. 7 clearly shows that the EIS results were well fitted to the equivalent circuit. From Table 2, it can be seen that the values of R_f and R_{ct} increased, whereas the values of Y_0 that represents CPE_1 and CPE_2 decreased by increasing inhibitor concentrations, which suggests that the amount of inhibitor molecules adsorbed on the electrode surface gradually increased and consequently resulting in the decreasing of active sites necessary for the coupled dissolution reaction. The increasing of R_f indicates that the development of a compact protective film on the electrode surface by the inhibitor adsorption, thereby enhancing the corrosion resistance of carbon steel [15,17]. The decrease in the capacitance values (Y_{0-CPE_1}) may be related to the displacement of iron oxides and/or hydroxides existing on carbon steel surface by the adsorbed inhibitor molecules [14,15]. The reduction in values of $Y_{0\text{-}CPE_2}$ can be ascribed to a decrease in the dielectric constant or an increase in the double electric layer thickness due to the inhibitor adsorption on the electrode surface [59,60]. The increasing of R_{ct} indicates that the charge transfer reactions occurring in the protective film were strongly restricted by the adsorbed inhibitor molecules. This reflects that the structure of electrode surface is improved and the carbon steel gets more resistant to the chloride attack, consequently leading to the decrease of corrosion rate. Moreover, by carefully examining the data listed in Tables 1 and 2, it can be seen that the values of η_{EIS} are very close to those of η_{LPR}, suggesting that they are in good agreement.

3.2. FTIR spectroscopy analysis

The electrochemical experiments showed that the inhibition effect of inhibitor is strongly related to its adsorption behavior on the carbon steel surface. For determining the presence of inhibitor on the sample surface, Fig. 9 displays the FTIR reflection spectra for carbon steel specimens after 3 days immersion in test solutions without and with 0.76 mM inhibitor, as well as the spectrum for pure HASI. It can be seen that in blank solution, only CO_2 bands at 2337 and 2360 cm^{-1} were detected on the surface of carbon steel [27,62]. By comparison, we find that the majority of the bands observed in the spectra of carbon steel samples immersed in solution with the inhibitor closely resemble those appearing in the pure HASI spectra. The bands at 2920 and 2850 cm^{-1} can be assigned to the $-CH_2-$ asymmetric and symmetric stretching vibrations, respectively [63,64]. These results indicate that the aliphatic hydrocarbon chain in the inhibitor molecule did not participate in the adsorption process of inhibitor. However, it is noticeable that there are some distinctive differences between the adsorbed inhibitor spectra and that of the pure HASI: (i) the band at 1651 cm^{-1}, as the characteristic stretching vibration of C=N in the imidazoline ring [64,65], was not observed in the spectra of adsorbed

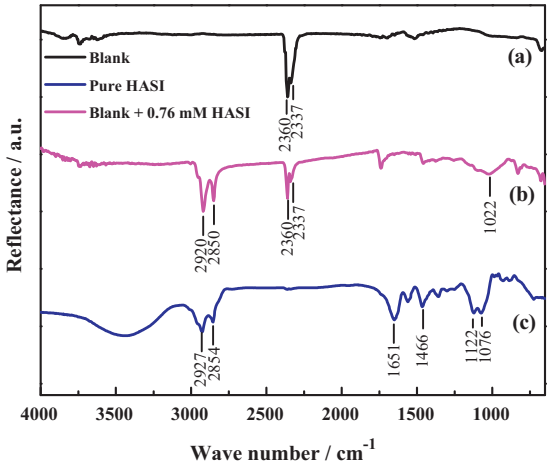

Fig. 9. FTIR spectra of pure HASI and carbon steel surface after 3 days immersion in 5% NaCl sat. $Ca(OH)_2$ solutions without and with 0.76 mM inhibitor: (a) Blank; (b) with inhibitor; (c) pure HASI.

inhibitor, confirming that there is the chemisorptions of imidazoline ring at carbon steel surface, (ii) the bands appeared at 1466, 1122 and 1076 cm^{-1} in the spectra of pure HASI, assigned to the C–N stretching vibrations, suffered the major loss in intensity and shifted to the lower wave numbers in the spectra of adsorbed inhibitor, suggesting that there is the strong adsorption interaction between the inhibitor molecules and the iron and/or iron oxides on carbon steel surface [64–66]. These facts reveal that the nitrogen atoms in imidazoline ring as the active centers participated in the adsorption process. Thus, it can be concluded that the inhibitor HASI is really present on the carbon steel surface by the adsorption.

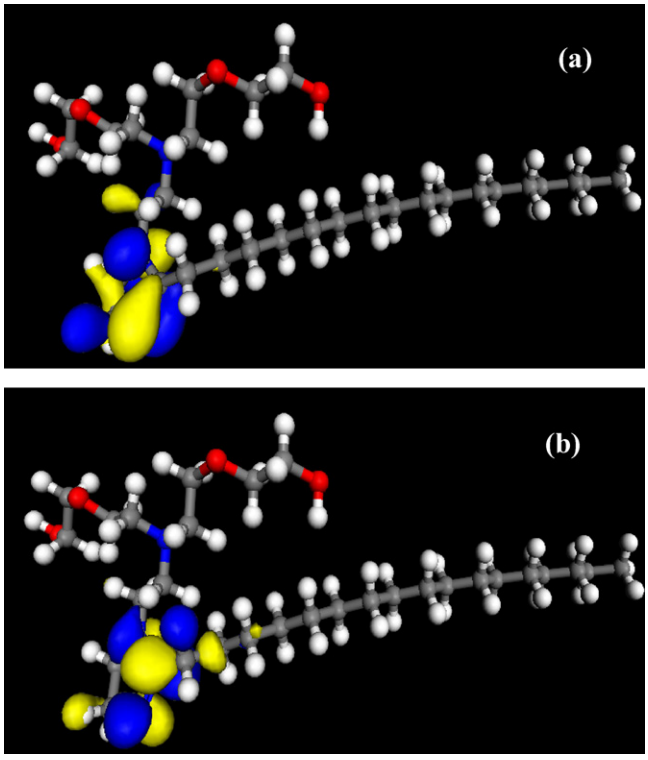

Fig. 10. Frontier orbital distribution of HASI molecule: (a) HOMO and (b) LUMO.

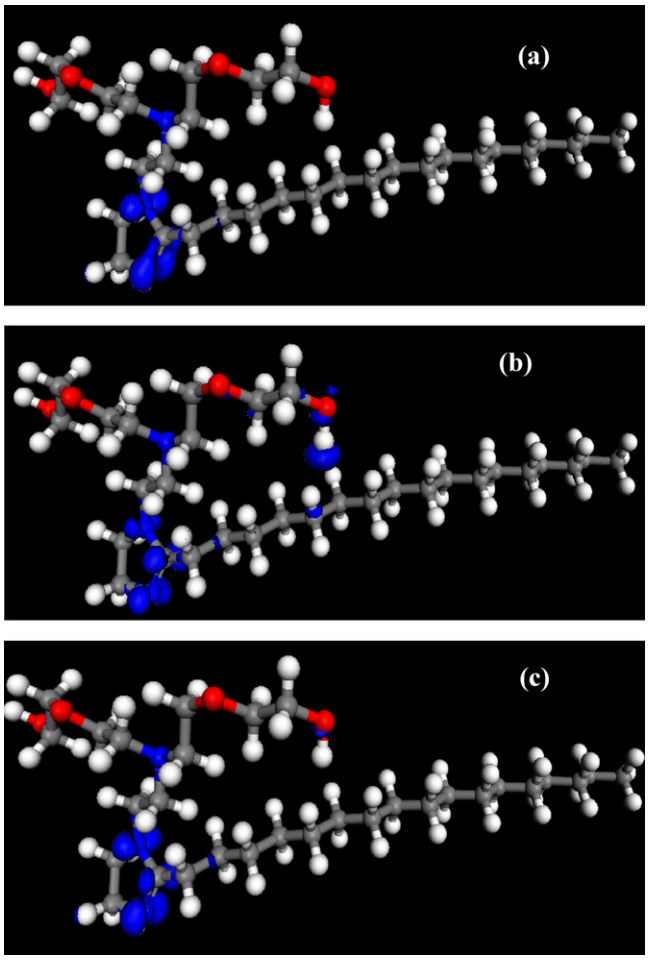

Fig. 11. Fukui function distribution: (a) Fukui function for electrophilic attack (f^-); (b) Fukui function for nucleophilic attack (f^+); (c) Fukui function for radical attack (f^0).

3.3. Quantum chemical calculation and molecular dynamic simulation

For further understanding the interactions between the inhibitor molecules and the carbon steel surfaces, the quantum chemical calculation and molecular dynamic simulation were performed. The optimized molecular structure of inhibitor is shown in Fig. 1. Fig. 10 presents the localization of the highest occupied molecular orbital (HOMO) and lowest unoccupied molecular orbital (LUMO), respectively.

According to the frontier molecular orbital theory, the formation of a transition state is due to an interaction between frontier orbitals (HOMO and LUMO) of reacting species. HOMO is often associated with the electron donating ability of a molecule, whereas LUMO indicates its ability to accept electrons. As can be seen from Fig. 10, the HOMO is distributed over the entire imidazoline moiety due to the presence of lone electron pairs in the nitrogen atoms and the delocalization of π-electrons in the imidazoline ring, which indicates that the preferred active sites for an electrophilic attack are located within the region around nitrogen atoms belonging to the imidazoline ring. The LUMO is mainly located on the N=C–N region in the imidazoline ring, which reveals that the preferred active sites for a nucleophilic attack are located in the N=C–N region. These results suggest that the N=C–N region in the imidazoline ring is the probable reactive site for the adsorption of inhibitor on the carbon steel surface. It has been found that the adsorption of an inhibitor on metal surface can occur on the basis of donor–acceptor interactions

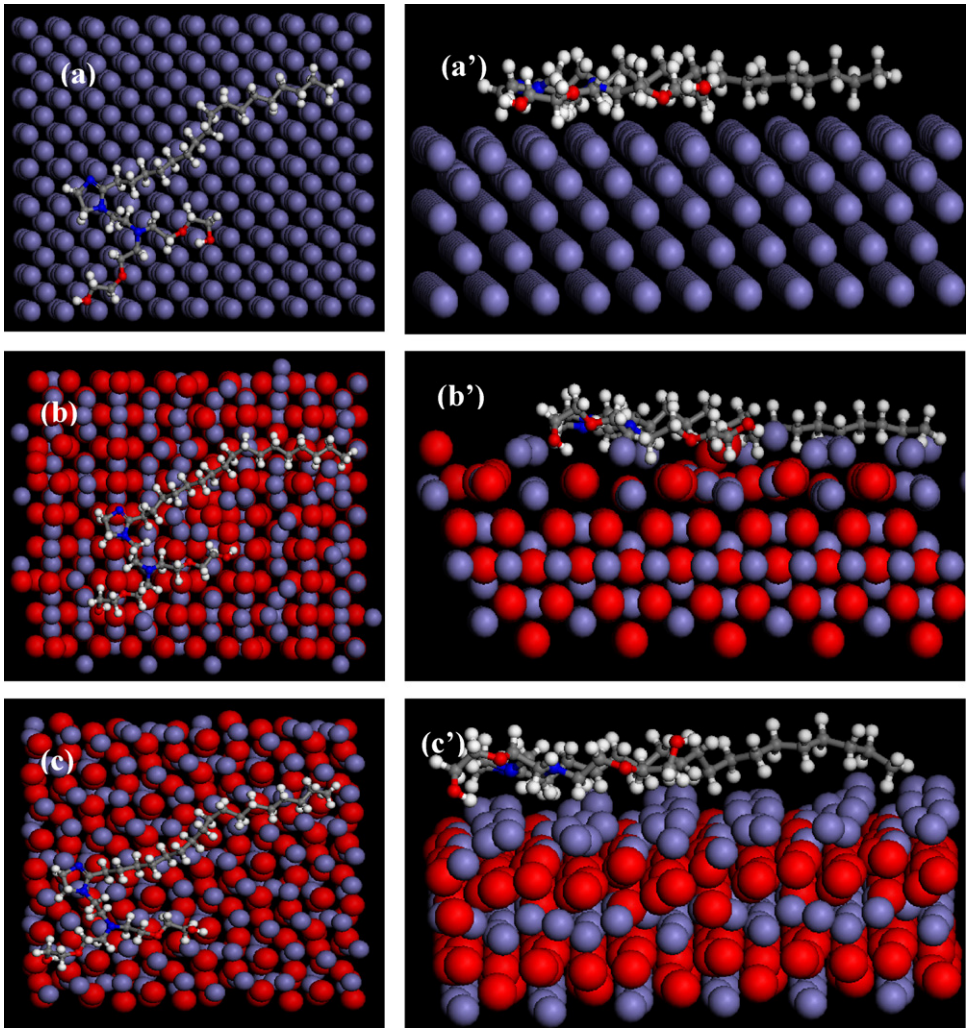

Fig. 12. Location of adsorbed inhibitor molecule on (a) Fe, (b) Fe_3O_4 and (c) Fe_2O_3 surfaces, respectively. The left is top view, and the right is side view.

between the lone electron pairs in heteroatoms together with the π-electrons of heterocyclic compound and the vacant d orbital of the metal surface atoms [45,67–69]. Thus, unoccupied d orbital of iron atom can accept electrons from the inhibitor molecule to form coordinate bonds. In addition, the inhibitor molecule can accept electrons from the iron atom with its anti-bonding orbitals to form back-donation bonds.

In order to further determine the local reactivity of functional groups in the inhibitor molecule, three kinds of Fukui functions (i.e. f^+, f^- and f^0) were also calculated and depicted in Fig. 11. For simplicity, only the calculated Fukui functions and the atomic charges over the nitrogen (N), oxygen (O) and carbon (C) atoms in the imidazoline ring are listed in Table 3.

The Fukui function is defined as the first derivative of the electronic density $\rho(\vec{r})$ with respect to the number of electrons (N) in a constant external potential $\nu(\vec{r})$ [70]:

$$f(\vec{r}) = \left(\frac{\partial\rho(\vec{r})}{\partial N}\right)_{\nu(\vec{r})} \tag{4}$$

By finite difference approximation, Fukui index can be derived as follows [36]:

$$f_k^+ = q_k(N+1) - q_k(N) \quad \text{(for nucleophilic attack)} \tag{5}$$

$$f_k^- = q_k(N) - q_k(N-1) \quad \text{(for electrophilic attack)} \tag{6}$$

$$f_k^0 = \frac{q_k(N+1) - q_k(N-1)}{2} \quad \text{(for radical attack)} \tag{7}$$

These Fukui functions determine the direction of the electron transfer in the interactions between the adsorbed inhibitor molecules and the metal surfaces.

As can be seen from Table 3, the nitrogen and oxygen as well as some carbon atoms possess the excess of negative charge. Among the nitrogen atoms, the highest negative charge is located on the N18 and N20 in the imidazoline ring, while among oxygen atoms the highest negative charge is found in O31 and O37. It is confirmed that the more negative the atomic charges of the adsorbed center, the more easily the atom donates its electrons to the unoccupied orbital of metal [37,71]. Therefore, these atoms with excess negative charge should be the active adsorption sites. However, it should be noted that due to the passivation effect of H atom, the reactivity of O atoms will be reduced [72]. Thus, the N18 and N20 may be the most active adsorption sites.

Further analysis of Fukui functions (Fig. 11) shows that the N18 and N20 in the imidazoline ring are the most susceptible sites for the electrophilic attacks as they present the highest values of f^-, 0.178 for N18 and 0.098 for N20 (Table 3), respectively. On the other hand, N18 and C19 are the most susceptible sites for the nucleophilic attacks. These sites present the highest values of f^+, which are 0.090 for N18 and 0.085 for C19. Moreover, the oxygen atoms in the hydrophilic side chain have lower values of Fukui indices. It

Table 3
Calculated Mulliken Fukui functions and atomic charges for the part atoms of inhibitor molecule.

Atom	f^-	f^+	f^0	Charge	Atom	f^-	f^+	f^0	Charge
N18	0.178	0.090	0.134	−0.450	N25	0.004	0.003	0.004	−0.382
C19	0.072	0.085	0.078	0.334	O28	0.011	0.013	0.012	−0.493
N20	0.098	0.014	0.056	−0.424	O31	0.011	−0.010	0.000	−0.563
C21	−0.034	−0.018	−0.026	−0.069	O34	0.012	0.005	0.009	−0.497
C22	−0.040	−0.022	−0.031	−0.081	O37	0.006	0.005	0.006	−0.561

Table 4
The interaction energy of inhibitor molecules with Fe, Fe_2O_3 and Fe_3O_4 surfaces.

Species	E_{inter} (kJ mol^{-1})
Fe/HASI	−284
Fe_2O_3/HASI	−157
Fe_3O_4/HASI	−226

has been found that the sites with the highest values of f^+ and f^- in molecular structure are the most susceptible sites for the nucleophilic and electrophilic attacks, respectively [72–74]. Therefore, it can be concluded that the N=C–N region in the imidazoline ring is the most active reaction site, and the adsorption of inhibitor as neutral molecules on the carbon steel surface can occur directly by sharing of electrons between the nitrogen atoms and iron atoms, in which involving the displacement of water molecules from the metal surface.

The molecular dynamic simulation can reasonably predict the most favourable configuration of the adsorbed inhibitor molecules on metal surface [30,73]. Considering the presence of iron oxides (such as Fe_2O_3 and Fe_3O_4) on the carbon steel surface in alkaline solution, so we choose three typical surfaces, i.e. Fe (1 0 0), F_2O_3 (1 1 0) and F_3O_4 (1 0 0) to simulate the adsorption behavior of inhibitor molecule. Fig. 12 displays the configurations of adsorbed inhibitor molecules on Fe, Fe_3O_4 and Fe_2O_3 surfaces, respectively. The calculated interaction energies (E_{inter}) according to the following equation [73] are listed in Table 4.

$$E_{inter} = E_{bond} - E_{nonbond} \quad (8)$$

where E_{bond} is the total energy of system after the adsorption of inhibitor molecule on the metal surface and $E_{nonbond}$ is the sum of the energy of metal surface and the inhibitor molecule before adsorption.

It is clearly observed from Fig. 12 that the inhibitor molecules were adsorbed in nearly parallel mode to the three typical surfaces so as to maximize its contact with the metal surface. This adsorption mode can be attributed to the strong interaction between the imidazoline ring and the metal surface. As stated above, N atoms in the imidazoline ring can offer electrons to the unoccupied d orbital of iron to form coordinate bonds, and anti-bonding orbital of π-electrons in the imidazoline ring can also accept the electrons from d orbital of iron to form feedback bonds [67–69]. In addition to the chemical interaction just described, the physical interaction between the inhibitor molecules and the metal surfaces driven by the van der Waals dispersion forces may be also contribute to the net molecule surface attraction since the strength of physical interaction generally scales with the size of the molecule [75,76].

Table 4 apparently shows that the interaction energy between the inhibitor molecules and Fe atoms presented the lowest value of −284 kJ mol^{-1}, followed by the Fe_3O_4 with −226 kJ mol^{-1} and Fe_2O_3 with −157 kJ mol^{-1}. This indicates that strong adsorption interactions occurred between the inhibitor molecules and the three different surfaces, yet the adsorption on the Fe surface was the most stable, and on the Fe_2O_3 surface was the least. This also gives a reasonable explanation why only Fe_3O_4 was detected on the carbon steel surface after the addition of an inhibitor.

4. Conclusions

(1) The inhibitor (HASI) has shown good inhibition performance for the corrosion of carbon steel in alkaline chloride solution. The inhibition effect increased with increasing concentrations of inhibitor.
(2) The electrochemical measurements show that the compound acts as a cathodic type inhibitor through forming a protective adsorption film to suppress dominantly the cathodic reduction of oxygen.
(3) Quantum chemical calculation results reveal that the nitrogen atoms belonging to the imidazoline ring are the most active adsorption sites by which the inhibitor molecules can directly adsorb onto carbon steel surface via the sharing of electrons with iron atoms.
(4) The MD simulation suggests that HASI molecules adsorb on metal surface in the planar manner with the higher negative interaction energy and the adsorption stability decreases in the following order Fe > Fe_3O_4 > Fe_2O_3.
(5) Data obtained from experiments along with the quantum chemical calculation and MD simulation results can provide a more complete scheme of the interactions between the inhibitor molecules and the metal surfaces.

Acknowledgements

The authors gratefully acknowledge the financial support from the National Natural Science Foundation of China (Grant No. 51071161) and the National Key Technology R&D Program (Grant No. 2007BAB27B03). We also thank Ph. Y.J. Wang for his help in the quantum chemical calculation and molecular simulation.

References

[1] L. Fedrizzi, F. Azzolini, P.L. Bonora, Cement Concrete Res. 35 (2005) 551.
[2] S. Fajardo, D.M. Bastidas, M. Criado, M. Romero, J.M. Bastidas, Constr. Build. Mater. 25 (2011) 4190.
[3] A.A. Gürten, K. Kayakirilmaz, M. Erbil, Constr. Build. Mater. 21 (2007) 669.
[4] F. Bolzoni, G. Fumagalli, L. Lazzari, M. Ormellese, M.P. Pedeferri, in: M. Raupach, B. Elsener, R. Polder, J. Mietz (Eds.), Corrosion of Reinforcement in Concrete: Mechanisms, Monitoring, Inhibitors and Rehabilitation Techniques, 1st ed., Woodhead Publishing Limited, Cambridge, England, 2007, p. 185.
[5] T.A. Söylev, C. McNally, M. Richardson, Cement Concrete Res. 37 (2007) 972.
[6] B. Elsener, E. Zurich, in: M. Raupach, B. Elsener, R. Polder, J. Mietz (Eds.), Corrosion of Reinforcement in Concrete: Mechanisms, Monitoring, Inhibitors and Rehabilitation Techniques, 1st ed., Woodhead Publishing Limited, Cambridge, England, 2007, p. 170.
[7] U. Angst, B. Elsener, C.K. Larsen, Ø. Vennesland, Cement Concrete Res. 39 (2009) 1122.
[8] S.M.A. El Haleem, S.A. El Wanees, E.E.A. El Aal, A. Diab, Corros. Sci. 52 (2010) 292.
[9] G. Batis, P. Pantazopoulou, A. Routoulas, Cement Concrete Compos. 25 (2003) 371.
[10] T.A. Söylev, M.G. Richardson, Constr. Build. Mater. 22 (2008) 609.
[11] L.B. Mechmeche, L. Dhouibi, M. Ben Ouezdou, E. Triki, F. Zucchi, Cement Concrete Compos. 30 (2008) 167.
[12] N. Etteyeb, L. Dhouibi, H. Takenouti, M.C. Alonso, E. Triki, Appl. Electrochim. Acta 52 (2007) 7506.
[13] S.Y. Qian, D. Cusson, Cement Concrete Compos. 26 (2004) 217.
[14] H.E. Jamil, A. Shouriri, R. Boulif, C. Bastos, M.F. Montemor, M.G.S. Ferreira, Electrochim. Acta 49 (2004) 2753.
[15] H.E. Jamil, M.F. Montemor, R. Boulif, A. Shouriri, M.G.S. Ferreira, Electrochim. Acta 48 (2003) 3509.

[16] O.T. de Rincon, O. Perez, E. Paredes, Y. Caldera, C. Urdaneta, I. Sandoval, Cement Concrete Compos. 24 (2002) 79.
[17] L. Valek, S. Martinez, D. Mikulić, I. Brnardić, Corros. Sci. 50 (2008) 2705.
[18] J. Telegdi, M.M. Shaglouf, A. Shaban, F.H. Kármán, I. Betráti, M. Mohai, E. Kálmán, Electrochim. Acta 46 (2001) 3791.
[19] J.J. Fu, S.N. Li, L.H. Cao, Y. Wang, L.H. Yan, L.D. Lu, J. Mater. Sci. 45 (2010) 979.
[20] W. Durnie, R. De Marco, A. Jefferson, B. Kinsella, J. Electrochem. Soc. 146 (1999) 1751.
[21] M. Ormellese, M. Berra, F. Bolzoni, T. Pastore, Cement Concrete Res. 36 (2006) 536.
[22] M. Ormellese, L. Lazzari, S. Goidanich, G. Fumagalli, A. Brenna, Corros. Sci. 51 (2009) 2959.
[23] X. Zhou, H. Yang, F. Wang, Electrochim. Acta 56 (2011) 4268.
[24] F. Wombacher, U. Maeder, B. Marazzani, Cement Concrete Compos. 26 (2004) 209.
[25] M.M. Mennucci, E.P. Banczek, P.R.P. Rodrigues, I. Costa, Cement Concrete Compos. 31 (2009) 418.
[26] N. Nakayama, A. Obuchi, Corros. Sci. 45 (2003) 2075.
[27] N. Nakayama, Corros. Sci. 42 (2000) 1897.
[28] G. Batis, A. Routoulas, E. Rakanta, Cement Concrete Compos. 25 (2003) 109.
[29] A. Rosenberg, Corrosion 56 (2000) 986.
[30] U. Maeder, in: R.N. Swamy (Ed.), Corrosion and Corrosion Protection of Steel in Concrete, Sheffield Academic Press, Sheffield, UK, 1994, p. 851.
[31] B. Bavarian, L. Reiner, in: M. Raupach, B. Elsener, R. Polder, J. Mietz (Eds.), Corrosion of Reinforcement in Concrete: Mechanisms, Monitoring, Inhibitors and Rehabilitation Techniques, 1st ed., Woodhead Publishing Limited, Cambridge, England, 2007, p. 239.
[32] B. Elsener, M. Buechler, F. Stalger, H. Boehni, Corrosion 56 (2000) 727.
[33] W. Morris, M. Vazquez, Cement Concrete Res. 32 (2002) 259.
[34] F. Bolzzoni, G. Fumagalli, L. Lazzari, M. Ormellese, M.P. Pedeferri, in: M. Raupach, B. Elsener, R. Polder, J. Mietz (Eds.), Corrosion of Reinforcement in Concrete: Mechanisms, Monitoring, Inhibitors and Rehabilitation Techniques, 1st ed., Woodhead Publishing Limited, Cambridge, England, 2007, p. 211.
[35] G. Gece, Corros. Sci. 50 (2008) 2981.
[36] K.F. Khaled, Electrochim. Acta 55 (2010) 6523.
[37] K.F. Khaled, Electrochim. Acta 53 (2008) 3484.
[38] Y. Tang, X. Yang, W. Yang, Y. Chen, R. Wan, Corros. Sci. 52 (2010) 242.
[39] M.A. Amin, K.F. Khaled, Q. Mohsen, H.A. Arida, Corros. Sci. 52 (2010) 1684.
[40] J. Liu, W. Yu, J. Zhang, S. Hu, L. You, G. Qiao, Appl. Surf. Sci. 256 (2010) 4729.
[41] A. Rossi, G. Puddu, B. Elsener, in: M. Raupach, B. Elsener, R. Polder, J. Mietz (Eds.), Corrosion of Reinforcement in Concrete: Mechanisms, Monitoring, Inhibitors and Rehabilitation Techniques, 1st ed., Woodhead Publishing Limited, Cambridge, England, 2007, p. 44.
[42] M. Sánchez-Moreno, H. Takenouti, J.J. García-Jareño, F. Vicente, C. Alonso, Electrochim. Acta 54 (2009) 7222.
[43] M. Sánchez, J. Gregori, C. Alonso, J.J. García-Jareño, H. Takenouti, F. Vicente, Electrochim. Acta 52 (2007) 7634.
[44] M.B. Valcarce, M. Vázquez, Electrochim. Acta 53 (2008) 5007.
[45] E. Machnikova, K.H. Whitmire, N. Hackerman, Electrochim. Acta 53 (2008) 6024.
[46] F. Bentiss, M. Traisnel, M. Lagrenée, Corros. Sci. 42 (2000) 127.
[47] E.J. Calvo, D.J. Schiffrin, J. Electroanal. Chem. 243 (1988) 171.
[48] E.R. Vago, E.J. Calvo, J. Electroanal. Chem. 339 (1992) 41.
[49] E.R. Vago, E.J. Calvo, M. Stratmann, Electrochim. Acta 39 (1994) 1655.
[50] S. Joiret, M. Keddam, X.R. Nóvoa, M.C. Pérez, C. Rangel, H. Takenouti, Cement Concrete Compos. 24 (2002) 7.
[51] W.C. Baek, T. Kang, H.J. Sohn, Y.T. Kho, Electrochim. Acta 46 (2001) 2321.
[52] J. Flis, I.F. Kabulska, T. Zakroczymski, Electrochim. Acta 54 (2009) 1810.
[53] C. Gabrielli, S. Joiret, M. Keddam, J. Electrochem. Soc. 153 (2006) B68.
[54] M.B. Valcarce, M. Vázquez, Mater. Chem. Phys. 115 (2009) 313.
[55] J. Flis, T. Zakroczymski, J. Electrochem. Soc. 143 (1996) 2458.
[56] F. Mansfeld, Electrochim. Acta 35 (1990) 1533.
[57] J.J. Shim, J.G. Kim, Mater. Lett. 58 (2004) 2002.
[58] E. Boubour, R.B. Lennox, Langmuir 16 (2000) 7464.
[59] X. Wang, H. Yang, F. Wang, Corros. Sci. 52 (2010) 1268.
[60] M. Salasi, T. Shahourabi, E. Roayaei, M. Aliofkhazraei, Mater. Chem. Phys. 104 (2007) 183.
[61] C. Jeyaprabha, S. Sathiyanarayanan, G. Venkatachari, Electrochim. Acta 51 (2006) 4080.
[62] S. De Angelis Curtis, M. Kubiak, K. Kurdziel, S. Materazzi, S. Vecchio, J. Anal. Appl. Pyrolysis 87 (2010) 175.
[63] P.E. Laibinis, G.M. Whitesides, D.L. Allara, Y.-T. Tao, A.N. Parikh, R.G. Nuzzo, J. Am. Chem. Soc. 113 (1991) 7152.
[64] B.V. Appa Rao, M. Yakub Iqbal, B. Sreedhar, Electrochim. Acta 55 (2010) 620.
[65] E.-S.M. Sherif, A.M. El Shamy, M.M. Ramla, A.O.H. El Nazhawy, Mater. Chem. Phys. 102 (2007) 231.
[66] R.G. Parr, W. Yang, J. Am. Chem. Soc. 106 (1984) 4049.
[67] I.B. Obot, N.O. Obi-Egbedi, Corros. Sci. 52 (2010) 198.
[68] I.B. Obot, N.O. Obi-Egbedi, Corros. Sci. 52 (2010) 282.
[69] H. Ashassi-Sorkhabi, B. Shaabani, D. Seifzadeh, Electrochim. Acta 50 (2005) 3446.
[70] L.M.R. Valdez, A.M. Villafane, D.G. Mitnik, J. Mol. Struct.: THEOCHEM 713 (2005) 65.
[71] C.T. Wang, S.H. Chen, H.Y. Ma, C.S. Qi, J. Appl. Electrochem. 33 (2003) 179.
[72] M. Finšgar, A. Lesar, A. Kokalj, I. Milošev, Electrochim. Acta 53 (2008) 8287.
[73] B. Gómez, N.V. Likhanova, M.A.D. Aguilar, O. Olivares, J.M. Hallen, J.A. Martínez-Magadán, J. Phys. Chem. A 109 (2005) 8950.
[74] A. Lalitha, S. Ramesh, S. Rajeswari, Electrochim. Acta 51 (2005) 47.
[75] D.J. Lavrich, S.M. Wetterer, S.L. Bernasek, G. Scoles, J. Phys. Chem. B 102 (1998) 3456.
[76] S.M. Wetterer, D.J. Lavrich, T. Cummings, S.L. Bernasek, G. Scoles, J. Phys. Chem. B 102 (1998) 9266.